Chemical Science

Accepted Manuscript

This article can be cited before page numbers have been issued, to do this please use: S. Bhunia, A. Rana, S. G. Dey, A. Ivancich and A. Dey, *Chem. Sci.*, 2020, DOI: 10.1039/C9SC04388H.

ROYAL SOCIETY OF CHEMISTRY

rsc.li/chemical-science

View Article Online
DOI: 10.1039/C9SC04388H

A Designed Second-Sphere Hydrogen-bond Interaction That Critically Influences The O–O Bond Activation for Heterolytic Cleavage in Ferric Iron-Porphyrin Complexes

Sarmistha Bhunia[1], Atanu Rana[1], Somdatta Ghosh Dey[1], Anabella Ivancich[2*], Abhishek Dey[1*]*

[1] Department of Inorganic Chemistry, Indian Association for the Cultivation of science, Kolkata, India, 700032

[2] CNRS, Aix-Marseille Univ, Laboratoire de Bioénergétique et Ingénierie des Protéines (UMR 7281), IMM FR3479, Marseille, France.

* Corresponding authors:

Email: icad@iacs.res.in

aivancich@imm.cnrs.fr

View Article Online
DOI: 10.1039/C9SC04388H

Abstract

Heme hydroperoxidases catalyze the oxidation of substrates by H_2O_2. The catalytic cycle involves the formation of a highly oxidizing species known as Compound I, resulting from the two-electron oxidation of the ferric heme in the active site of the resting enzyme. This high-valent intermediate is formed upon facile heterolysis of the O-O bond in the initial Fe^{III}-OOH complex. Heterolysis is assisted by the histidine and arginine residues present in the heme distal cavity. This chemistry has not been successfully modeled in synthetic systems up to now. In this work, we have used a series of Fe^{III} porphyrin complexes (Fe^{III}L2(Br), Fe^{III}L3(Br) and Fe^{III}MPh(Br)) with covalently attached pendent basic groups (pyridine, primary amine) mimicking the histidine and arginine residues in the distal-pocket of natural heme enzymes. The presence of pendent basic groups, capable of 2nd sphere hydrogen bonding interactions, lead to almost 1000-fold enhancement in the rate of compound I formation from peracids relative to analogous complexes without these residues. The short-lived Compound I intermediate formed at cryogenic temperatures could be detected using UV-vis electronic absorption spectroscopy and also trapped to be unequivocally identified by 9-GHz EPR spectroscopy at 4K. The broad (2000 G) and axial EPR spectrum of an exchange-coupled oxoferryl-porphyrin radical species, the [Fe^{IV}=O $Por^{\bullet+}$] with $g_{\perp}^{eff} = 3.80$ and $g_{||}^{eff} = 1.99$ was observed upon reaction of Fe^{III}L3-Br) porphyrin complex with *m*-CPBA. The characterization of the reactivity of the Fe^{III} porphyrin complexes with the substrate in presence of oxidant like *m*-CPBA by UV-vis electronic absorption spectroscopy showed that they are capable of oxidizing two equivalents of inorganic and organic substrate(s) like Ferrocene, 2,4,6-tritertiary butyl phenol and o-phenylenediamine. These oxidations are catalytic with a turnover number (TON) as high as 350. Density Functional Theory (DFT) calculations show that the mechanism of O-O bond activation by 2nd sphere hydrogen bonding interaction from these pendent basic groups, which are protonated by the peracid, involves polarization of the O-O σ-bond, leading to lowering of the O-O σ*-orbital allowing enhanced back bonding from the iron center. These results demonstrate how inclusion of 2nd sphere hydrogen bonding interaction can play a critical role in O-O bond heterolysis.

View Article Online
DOI: 10.1039/C9SC04388H

Introduction

Factors that can affect heterolytic O-O bond cleavage of metal peroxide species are of great contemporary interest.[1, 2] Heterolysis of metal peroxides generate high-valent metal oxo species which are very reactive and have been demonstrated to be able to catalyze oxidation of inert organic compounds, processes that are of highly relevant to the chemistry community.[3-7] The inspiration for such chemistry is derived from naturally occurring heme metalloenzymes (monofunctional peroxidases,[8] catalases,[9] bifunctional catalase-peroxidases (KatGs),[10] cyt P450 monooxygenases[11] and P450 peroxygenases[12]) where detailed biochemical experiments heralded the presence of 1st and 2nd coordination sphere residues in the heme active site that are essential for the generation of high-valent catalytic intermediates. The resting state of peroxidases, peroxygenases and catalases is the ferric oxidation state of the heme iron and the catalytically-competent high-valent intermediate [Fe^{IV}=O $Por^{\bullet+}$], Compound I, is formed by the reaction with hydrogen peroxide or alternative two-electron oxidants. Upon reaction with substrates, the one-electron reduction of Compound I results in the formation of the Fe^{IV}=O species known as Compound II, which undergoes further one electron reduction and regains back the resting ferric state.[13] The Compound I intermediate is the strongest oxidant in the catalytic cycle of peroxidases which are involved in several activities like biosynthesis of hormones (cycloperoxidases), defense against pathogens (myeloperoxidase and horseradish peroxidase) and regulating cellular oxidative stress (CcP and GSH peroxidase).[14, 15] The oxidizing ability of high valent intermediates makes it valuable to the chemical industry as it can catalyze difficult chemical oxidations relevant to synthesis of fine chemicals, waste water decontamination of toxic phenol and polymerization.[16, 17] The ferric hydroperoxide (Fe^{III}-OOH) intermediate, known as Compound 0 [18, 19], is the very short-lived species preceding the formation of Compound I in all hydroperoxidases [20, 21] A Histidine residue is involved in the protonation of Compound 0 in the active site of peroxidases [22-24] Histidine acts as a base initially deprotonating the proximal oxygen atom of hydroperoxide bound to the heme iron, and then transfers the proton to the distal oxygen atom as an acid catalyst to facilitate the heterolytic O-O bond cleavage and water release, assisted by an arginine residue, leaving the oxygen atom bound to the iron (Figure 1).[20, 24-27]

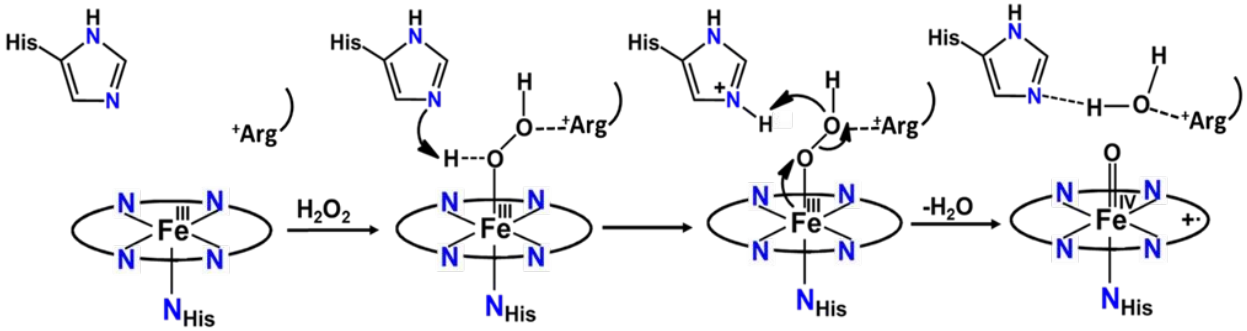

Figure 1. Mechanism for the formation of Compound I intermediate in peroxidases, involving the His and Arg residues of the heme distal side.[15,27,28]

View Article Online
DOI: 10.1039/C9SC04388H

The arginine residue, being positively charged at neutral pHs likely helps in polarization of the O-O bond and promotes heterolysis as its mutation leads to a two orders of magnitude reduction in the rates.[28] This combined role of histidine and arginine residues in the heme distal side exerts "Pull-effect" and results in facile heterolytic cleavage of the O-O bond.[20, 24, 26, 29] Such a "Pull effect" is also exhibited by other peroxidases with similar distal acid-base residue.[30-32] Arginine hydrogen binds to the ferryl oxygen atom of Compound I and thus may stabilize the high valent reactive intermediates.[28] The arginine residue enhances the binding of substrate to the peroxidase active site as its mutation increases the K_M for the substrate.[33-35] Peroxidases such as HRP show minimal heme degradation during catalysis, mostly happening in the presence of very high molar excess of oxidant. [36, 37]

Over the last several decades, several synthetic systems were designed for the investigation of the "Push-Pull" effect and the formation of Compound I was examined using various oxidants.[38-41] Watanabe and coworkers monitored the formation of Compound I in organic medium with peracids in a series of synthetic iron-porphyrins by varying the substituents in their meso phenyl rings and also using substituted axial imidazole ligands.[42] Groves and coworkers demonstrated that the nature of the bond cleavage process can be controlled by changing the polarity of solvent in some systems.[43, 44] Fujii and coworkers examined the spin coupling interaction between the ferryl iron and the porphyrin π-cation radical using EPR spectroscopy to probe the a_{1u}/a_{2u} character of the high-valent intermediates in several iron porphyrins with different substituents in meso phenyl rings as well as β-pyrroles.[45] Nocera and co-workers introduced hanging carboxylic acid residues to impose 2nd sphere interactions with reaction intermediates mimicking the distal residues in the protein active site which promote heterolytic bond fission.[46, 47] Unfortunately, the reported rates for O-O bond heterolysis did not indicate a substantial role of the pendent carboxylic acids.[46] In a very recent work, incorporation of pendent amine group in the 2nd coordination sphere of non heme iron complex has been reported to form selectively the Fe^{IV}=O intermediate via heterolytic O-O bond cleavage with lower activation energy barrier by the reaction of non-heme Fe(II) complex with H_2O_2.[5]

To date, the role of the histidine residue as acid-base catalyst in the distal site of peroxidases remains to be successfully modeled in any synthetic heme-based model system. Peroxidases generally oxidize organic phenols and aromatic amines using an outer sphere electron transfer and oxidation of substrates like epoxidation and sulfoxidation, traditionally performed by monoxygenases, are reported.[48-53] So far, molecular mimics of the Compound I intermediate of peroxidases are reported to catalyze epoxidation and sulfoxidation with low turnover number or yield.[47, 54, 55] Yet, catalytic oxidation of phenols and amines, the typical substrates for peroxidases with significant turnover number have not been achieved.[56-58] This is particularly important as the hydroperoxidase activity is a key technology for degradation of organic contaminants in water. Thus, facile generation of a synthetic reactive intermediate mimicking Compound I to be used for catalytic transformations and retarding its self-degradation, is of interest to a broad community of chemists. Recently, mononuclear (ferric) iron porphyrins with pendent basic groups were reported (Fig. 2, B and C) which could reduce oxygen to water with greater than 95% selectivity at pH 7 with rates > 10^7 $M^{-1}s^{-1}$.[59] The origin of such high reactivity and much desired selectivity in

View Article Online
DOI: 10.1039/C9SC04388H

simple mononuclear iron porphyrin was proposed to originate from specific proton transfer to the distal oxygen, akin to peroxidases, of a putative ferric hydroperoxide species from the pendent basic groups which remains protonated at pH 7. These proposals were supported by DFT calculations.[59]

In this work, we have used a series of ferric iron porphyrin complexes with pendent basic groups covalently attached to the amine group of meso-phenyl ring (see Figure 2) in the tetraphenylporphyrin architecture, in order to investigate the rates of O-O bond heterolysis and to characterize the ensuing intermediates formed. Compound I is detected upon oxidation of these ferric iron porphyrin complexes with a peracid (*m*-chloroperbenzoic acid), as clearly shown by the stopped-flow kinetics and EPR spectroscopic characterization. Pyridine and amine, designed as pendent groups emulating the distal His residue in natural peroxidases (see Figure 1), translocate protons from the proximal to distal oxygen atom of bound *m*-chloroperbenzoic acid to facilitate the heterolytic cleavage pathway with much higher rates than the benzyl analogue (Fig. 2D, Fe^{III}MPh(Br)), a structurally analogous iron porphyrin without base, and also than any previously reported synthetic porphyrins thus with rates comparable to natural peroxidases. The results also suggest that the self-degradation of the Fe^{III} porphyrin catalyst was prevented, most likely by the hydrogen bonding interaction of the pendent base with the Fe^{IV}=O center of Compound I, thus allowing these synthetic hemes to efficiently catalyze the oxidation of organic and inorganic substrates using peracids. Density Functional Theory (DFT) calculations support the experimentally observed activation of a bound peroxide by pendent bases and help in developing a molecular orbital theory rationale of the elusive "pull effect".

Results and Discussion

The formation of high valent iron-oxo intermediate was examined for four iron (III) porphyrin model complexes (Fig. 2) e.g., Fe^{III}L2(Br) and Fe^{III}L3(Br) each containing a distinct pendent (basic) residue pyridine and aliphatic amine, respectively, Fe^{III}MPh(Br) containing mono benzyl group without additional basic residue and simple mononuclear iron porphyrin without any second sphere residue (Fe^{III}TPP(Br)) (Fig. 2). *m*-CPBA was used as oxidant. The pKa values of the pendent pyridine and amine groups in Fe^{III}L2(Br) (Fig. 2A) and Fe^{III}L3(Br) (Fig. 2B) complexes were determined to be 12.33 and 16.90, respectively in CH_3CN.[60] The reactions were monitored at sub-zero temperatures in a stopped-flow UV-vis electronic absorption spectrometer.

View Article Online
DOI: 10.1039/C9SC04388H

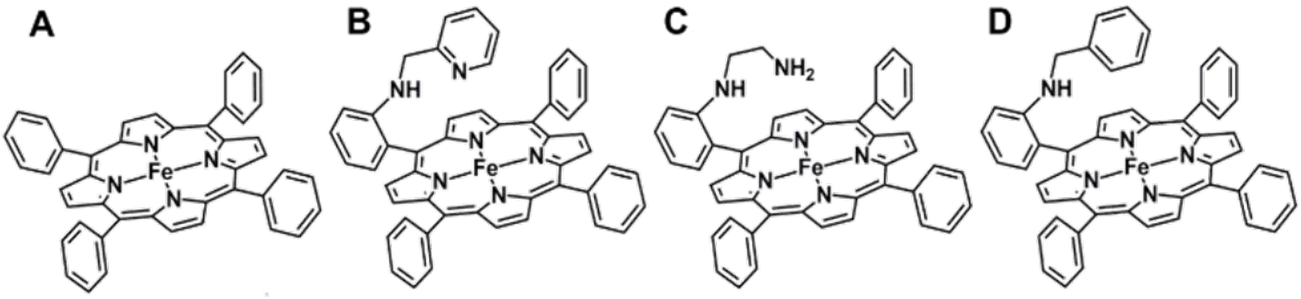

Figure 2. Molecular structures of iron-porphyrin complexes used in this study: A) Fe^{III}TPP, B) Fe^{III}L2, C) Fe^{III}L3 and D) Fe^{III}MPh.

Upon reaction of Fe^{III}L2(Br) with *m*-CPBA in dichloromethane (DCM) at -30ºC, the electronic absorption spectrum of the ferric state showed decrease in intensity of the Soret (417 nm) and charge transfer bands at 510 nm, 594 nm and 695 nm. In addition, a new and rather broad band centered at ca. 705 nm was also observed (Fig. 3A). Similar changes were observed for the Fe^{III}L3(Br) complex under the same conditions where a broad band appeared at ca. 726 nm (Fig. 3B). In the case of the Fe^{III}MPh(Br) complex, where no basic residue is present, a new broad band at ca. 705 nm (Fig. 3C) is observed. The broad charge transfer band at ~700 nm is consistent with the formation of the iron(IV)-oxo porphyrin cation radical intermediate, Compound I, previously reported in synthetic model complexes as well as in enzyme systems.[43, 46, 61-65]

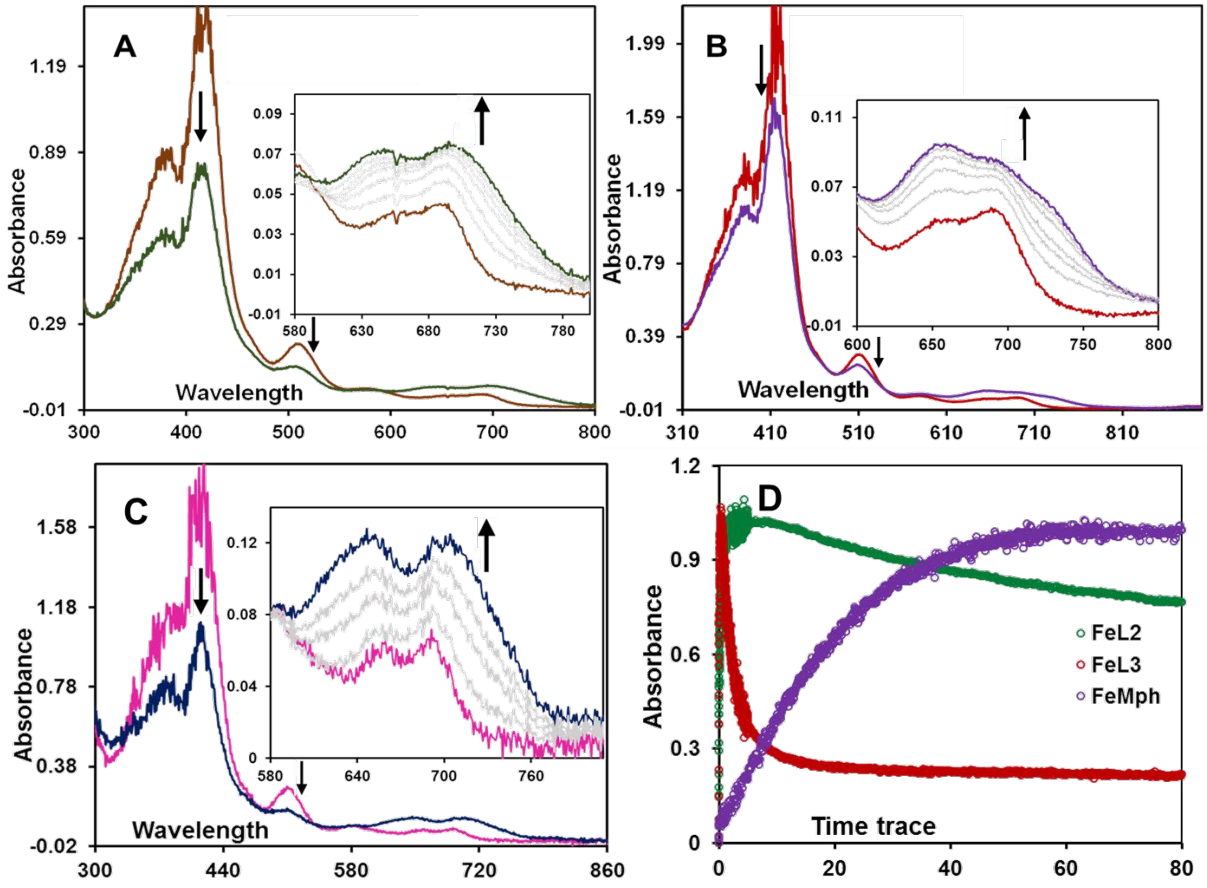

View Article Online
DOI: 10.1039/C9SC04388H

Figure 3. Stopped-flow absorption spectral changes after the reaction of 50 μM complexes A) $Fe^{III}L2(Br)$, B) $Fe^{III}L3(Br)$ and C) $Fe^{III}MPh(Br)$ with 200 μM *m*-CPBA in dichloromethane at -30ºC. In (A) Brown solid line: resting $Fe^{III}L2(Br)$ at the beginning of the reaction, Green line: the intermediate formed at 5 sec corresponding to $[Fe^{IV}=O\ Por^{\bullet+}]L2$; In (B) Red line : resting $Fe^{III}L3(Br)$ at the beginning of the reaction, violet line : the intermediate formed at 500 msec corresponding to $[Fe^{IV}=O\ Por^{\bullet+}]L3$; In (C) Pink line : resting $Fe^{III}MPh(Br)$ at the beginning of the reaction, blue line: the intermediate formed after 1 minute corresponding to $[Fe^{IV}=O\ Por^{\bullet+}]MPh$, Grey lines: the conversion as a function of time from resting iron(III)-porphyrins to intermediate species, after addition of *m*-CPBA. (D) Red circles: time trace of $Fe^{III}L3$ at 726 nm, Green circles: time trace of $Fe^{III}L2$ at 705 nm and violet circles: time trace of $Fe^{III}MPh$ at 705 nm.

The formation of 705 nm band of $Fe^{III}L2(Br)$ maximizes within 5 sec (Fig. 3D, green trace & S1A, red trace). The species is quite stable at -30°C and takes around 5 minutes for this band to disappear (Fig. S4B, blue trace). However, the formation of this band takes much longer time, i.e. around 1 min, in the case of $Fe^{III}MPh(Br)$ (Fig. 3D & S1C, violet trace). The absorbance at 726 nm band for $Fe^{III}L3(Br)$ maximizes within 500 ms (Fig. S1B, green trace) and decays by 10 sec (Fig. 3D, red trace & S4A, green trace) at -30ºC. The rate constants for the formation of Compound I are 21.67±1 s^{-1}, 67.6±2 $s^{-1}$and (8.5±1)×10^{-2} s^{-1} for $Fe^{III}L2(Br)$, $Fe^{III}L3(Br)$ and $Fe^{III}MPh(Br)$, respectively (Figure 4) at -30ºC (i.e. 243 K). A more than two orders of magnitude faster O-O bond heterolysis in $Fe^{III}L2$ and $Fe^{III}L3$ with respect to $Fe^{III}MPh$ provides definitive proof of the advantage of the pendent nitrogenous bases during heterolytic cleavage. The first order rate constants for these two complexes are even much higher than those for previously reported model complexes (Table 1). The rate constants for the decay of these bands are (3.2±0.5)×10^{-1} s^{-1} and (5±0.7)×10^{-3} s^{-1} for $Fe^{III}L2(Br)$ and $Fe^{III}L3(Br)$, respectively, obtained from the first order exponential fits to the absorbance vs time traces (Figure 4). Compound I intermediate for both of these complexes is converted to the corresponding Compound II ($Fe^{IV}=O$) species as indicated by the characteristic bands at 650 nm and 657 nm for $Fe^{III}L2(Br)$ and $Fe^{III}L3(Br)$, respectively, which is stable for several minutes at -30°C (Figure S3). Note that the formation and decay of Compound I can be fit using a kinetic model for consecutive reaction (Fig. S4) suggesting that the disproportionation of Compound II to form Compound I and ferric species is not observed here as has been reported for non-heme systems.[66-68]

View Article Online
DOI: 10.1039/C9SC04388H

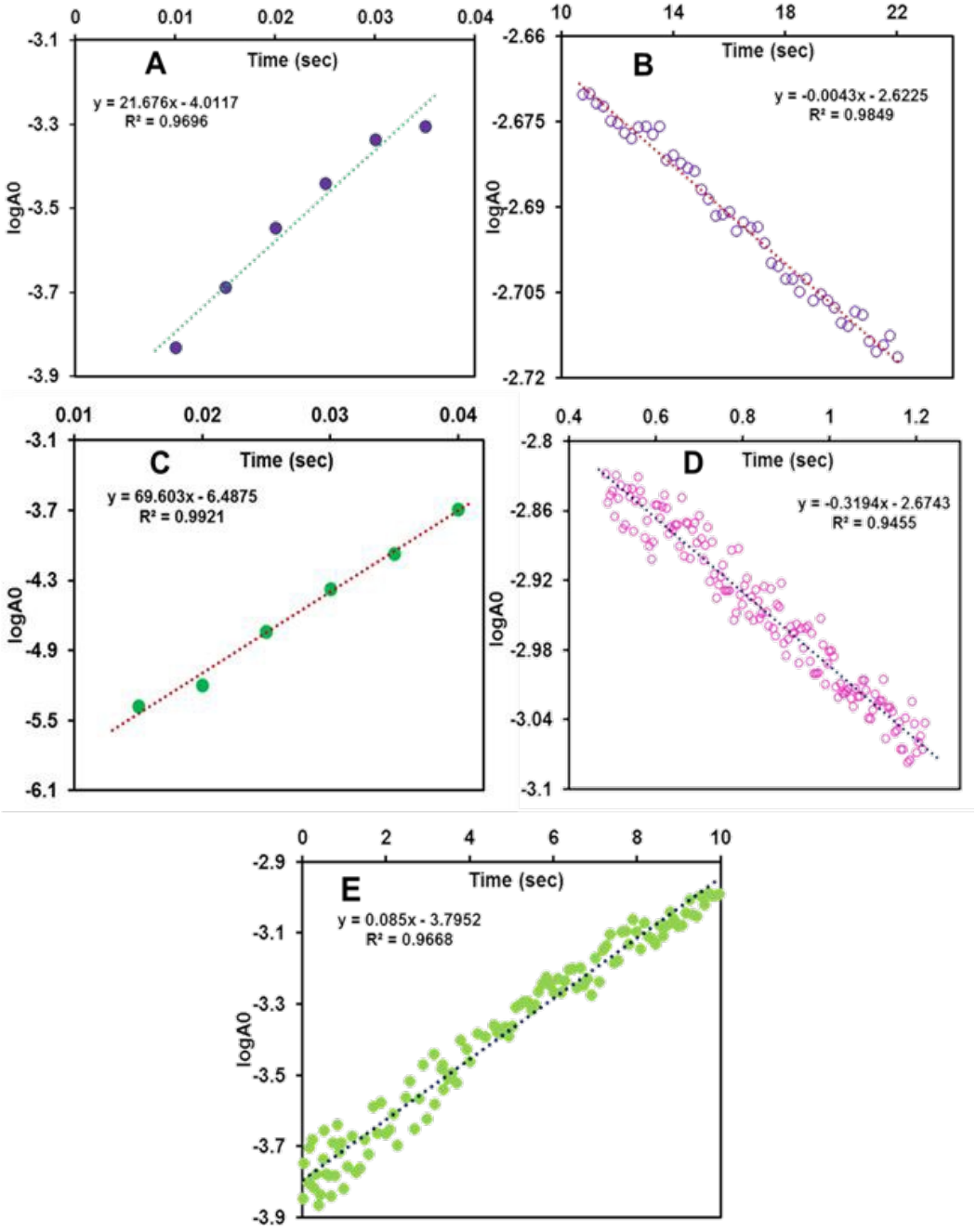

Figure 4. Linear Fit of initial logA0 vs time trace: Reaction of $Fe^{III}L2(Br)$ (50 µM) with 4eq *m*-CPBA (100 µM) in dichloromethane at -30°C leads to formation of Compound I intermediate (λmax = 710 nm) represented by blue circles (A) and decay of Compound I intermediate represented by purple circles (B). The first order rate constants obtained from the slopes of log A0 vs t plot for the formation and decay of Compound I are 21.67 s^{-1} and 0.004 s^{-1}, respectively. Reaction of $Fe^{III}L3(Br)$ (50 µM) with 8eq *m*-CPBA (200 µM) in dichloromethane at -30°C leads to the formation of Compound I intermediate (λmax = 726 nm) represented by green circles (C) and decay of Compound I intermediate indicated by pink circles (D). The first order rate constants obtained from the slopes of log A0 vs t plot for the formation and decay are 69.60 s^{-1} and 0.32 s^{-1}, respectively. (E) Reaction of $Fe^{III}Mph(Br)$

View Article Online
DOI: 10.1039/C9SC04388H

(50 μM) with 8eq *m*-CPBA (200 μM) in dichloromethane at -30°C leads to the formation of Compound I intermediate (λmax = 710 nm) represented by green circles. The first order rate constant (obtained from the slope of log A0 vs time plot) for Compound I formation is 0.085 s^{-1}.

Table 1: The rate of O-O heterolysis and the corresponding activation parameters

Catalyst	$k_{heterolysis}$ (s^{-1})	Temperature	$\Delta G^{\neq}$ (kcal/mol^{-1})	Ref
6a	16.6×10^{-3}	-80°C	12.78	41
6b	4×10^{-3}	-80°C	13.33	41
6d	3.94×10^{-3}	-40°C	16.19	41
6e	0.5×10^{-4}	-80°C	14.14	41
Fe^{III}TMP	$(6.5\pm1)\times10^{-3}$	-40°C	15.96±0.1	45
Fe^{III}(HPX-CO_2H)	$(6\pm3)\times10^{-3}$	-40°C	15.99±0.2	45
Fe^{III}(HPX-CO_2Me)	$(1\pm0.2)\times10^{-2}$	-40°C	15.76±0.1	45
Fe^{III}L2	21.67±1	-30°C	12.72±0.02	This work
Fe^{III}L3	69.6±2	-30°C	12.15±0.01	This work
Fe^{III}MPh	$(8.5\pm1)\times10^{-2}$	-30°C	15.08±0.05	This work
HRP	200-500s^{-1}	25°C	13-14	53,70
H42A/H42V	$(5\text{-}50)\times10^{-4}$	25°C	21±1	71,73

The molecular structures (6a, 6b, 6d and 6e) corresponding to ref. 41 are given in figure 6. Here, meta-chloroperbenzoic acid is used as oxidant for all the catalysts except for ref 53, 71 and 73 (where hydrogen peroxide is the oxidant).

The reaction of *m*-CPBA with Fe^{III}TPP(Br) under identical conditions did not show the formation of Compound I, rather it shows a very slow formation of isoporphyrin, a species isoelectronic with Compound I and an intermediate in heme degradation of heme oxygenase cycle , that has characteristic bands at 810 nm and 900 nm (Fig. 5A, red trace and Fig. S2) suggesting the decay pathway of the porphyrin macrocycle of Fe^{III}TPP(Br) consistent with previous literature (Scheme S1).[36, 62, 69] Alternatively, the Fe^{III}L2(Br) and Fe^{III}L3(Br) complexes form their high valent oxo species and decay to their resting ferric state in their reaction with mCPBA in contrast to Fe^{III}TPP(Br) (Fig. 5A). Note that minor and sluggish formation of isoporphyrin is detected in Fe^{III}L2(Br), Fe^{III}L3(Br) and Fe^{III}MPh(Br) as indicated by the absorption spectra and time traces of 800 nm and 900 nm band (Fig. 5A & 5B; Fig. S1A, S1B & S1C) and is likely due to competitive binding of *m*-CPBA at the open site of the porphyrin, which logically follows a Fe^{III}TPP-like reactivity (Fig. S2). Overall, it is clear that the pendent basic groups avoid degradation of the heme upon its reaction with peracids.

View Article Online
DOI: 10.1039/C9SC04388H

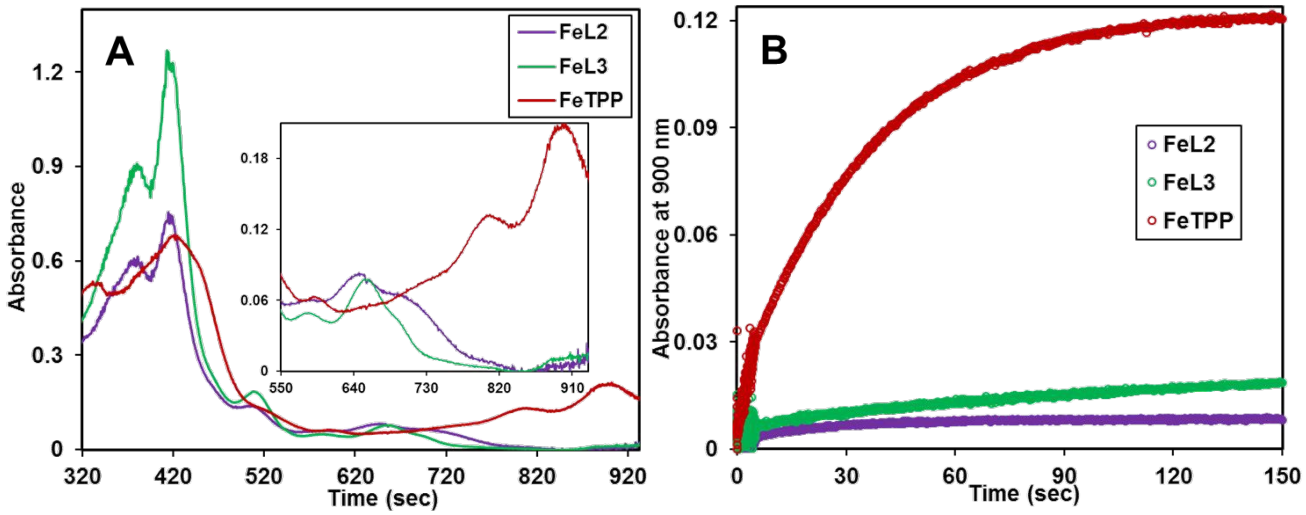

Figure 5. Rapid-scan electronic absorption spectra of the reaction of iron porphyrin complexes (50 µM) with 8 equivalent of meta-chloroperbenzoic acid (*m*-CPBA, 200 µM) in dichloromethane followed at -30°C. (A) Selected overlay spectra representing the intermediate species formed after 50 sec of the reaction, (B) Overlay of the time traces at 900 nm band with the formation of isoporphyrin species (λmax = 900 nm) for these three complexes (Fe^{III}TPP(Br) (red line), Fe^{III}L2(Br) (violet line) and Fe^{III}L3(Br) (green line)).

The rates of Compound I formation from ferric porphyrins via heterolysis of O-O bond of bound peracid (*m*-CPBA) are obtained at -30°C. Since, the kinetics for formation of the Compound I have been obtained at different temperature than previously reported metalloporphyrin systems, direct comparison of the rate constants are not possible (Figure 6, Table 1). The activation energies ($\Delta G^{\neq}$) for O-O bond heterolysis of Fe^{III}L2 and Fe^{III}L3 are obtained from the observed rates using Eyring equation and compared to those calculated for different model iron porphyrins (Table 1) from their reported rates.[42, 46] The lowest energy barrier attained is 12.78 kcal/mol for complex 6a (Figure 6) which fashions the most electron rich porphyrin ring among all of the synthetic models reported till date. The presence of large number of electron donating methoxy substituents in 6a makes it facile to undergo faster heterolytic O-O bond cleavage than any other meso substituted porphyrins as reported by Watanabe et al.[42] The $\Delta G^{\#}$ of O-O bond heterolysis exhibited by Fe^{III}L2(Br), Fe^{III}L3(Br) and Fe^{III}MPh(Br) are 12.72 ± 0.02 kcal/mol, 12.15 ± 0.01 kcal/mol and 15.08±0.05 kcal/mol, respectively. The activation energies of pendent base containing models match well with the earlier reported models (6a and 6b, Table 1). We have derived another two activation parameters i.e. $\Delta H^{\#}$ (2.34 ± 0.2 kcal/mol) and $\Delta S^{\#}$ (-44.60 ± 1cal mol^{-1} K^{-1}) from the linear Arrhenius plot of temperature dependent kinetic study for Compound I formation of Fe^{III}L2(Br). The remarkably low enthalpic barrier and large negative entropy of activation also support the facile O-O bond cleavage step. The $\Delta G^{\#}$ (13.03 ± 0.3 kcal/mol) is also determined from kinetics at different temperatures from the sum of $\Delta H^{\#}$ and $\Delta S^{\#}$ which is in good agreement to that obtained directly from first order rate constants using Eyring equation (details in SI). It is important to note that the $\Delta G^{\#}$ of O-O bond heterolysis is 3-4 kcal/mol lower in Fe^{III}L2 and Fe^{III}L3 relative to structurally analogous Fe^{III}MPh, Fe^{III}TMP and iron-hangman porphyrins which have pendent carboxylic acid/ester

View Article Online
DOI: 10.1039/C9SC04388H

groups (Table 1) directly establishing the efficacy of pendent basic groups in enhancement of heterolytic O-O bond cleavage rates. Additionally, the three times faster rate and 0.5 kcal/mol lower $\Delta G^{\#}$ of $Fe^{III}L3(Br)$ with an aliphatic amine (pk_a~16.9 in CH_3CN) than $Fe^{III}L2(Br)$ with a pyridine group (pk_a~12.33 in CH_3CN) suggest that the O-O bond heterolysis is favored by pendent amine groups having higher basicity than the peracid. Therefore, these residues can easily act as efficient acid-base catalyst and capable of deprotonating the distal oxygen atom of bound peracid and transferring it to distal oxygen atom that is necessary for the heterolysis. The rate of Compound I formation from *m*-CPBA in native HRP is 200-500 s^{-1} and two histidine mutants of HRP; H42A and H42V show 10^5-10^6 order lowering of rate i.e. (5-50)×10^{-4} s^{-1} at room temperature.[53, 70, 71] The corresponding activation energy barrier for HRP (~13-14 kcal/mol) is much lower than the histidine mutants (21±1 kcal/mol) and comparable to that achieved in these synthetic models $Fe^{III}L2(Br)$ and $Fe^{III}L3(Br)$. Thus, the "pull effect" in peroxidases is successfully mimicked in synthetic models including pendent basic groups (analogous to histidine residue) in the 2nd sphere of the iron porphyrin. Note that, mutation of the His42 residue in HRP leads to several orders of magnitude decrease in the rate of Compound I formation via O-O bond heterolysis,[27, 72, 73] which is reasonably captured in two orders of magnitude reduction in the rate of compound I formation in the FeMPh relative to FeL2 and FeL3.

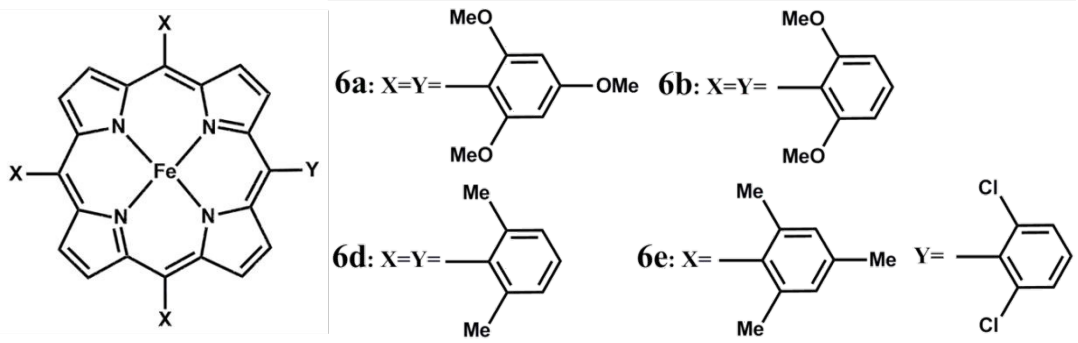

Figure 6. Structures of model iron-porphyrins referred in Table 1.

Identification of the high-valent intermediates by EPR spectroscopy.

To further identify and characterize the catalytically-relevant high-valent intermediates (Compound I and Compound II) proposed from the spectral changes in the electronic absorption spectra (Fig. 3 and Fig. S3), we applied 9-GHz cw-EPR spectroscopy at liquid helium temperatures, and monitored the reaction of the $Fe^{III}L3$ porphyrin complex with *m*-CPBA (both in dichloromethane). The reaction of the $Fe^{III}L3$ porphyrin complex with 10-fold molar equivalents of *m*-CPBA was done by manual mixing and directly in the quartz EPR tube placed in a *ca.* -100°C bath, in order to trap the short-lived intermediates. In particular, we aimed to characterize the short-lived intermediate assigned to Compound I, showing an electronic absorption CT band at 726 nm and appearing within 500 ms upon reaction of the $Fe^{III}L3$ Por complex with *m*-CPBA at -30ºC. The subsequent intermediate with an electronic absorption CT band at 657 nm, and that was assigned to Compound II, proved to be stable for several minutes at -30°C (Fig. S3).

View Article Online
DOI: 10.1039/C9SC04388H

The Fe^{III}L3 complex shows an axial EPR spectrum with observed g_{eff} values at $g_{\perp} = 6.04$ and $g_{\parallel} = 1.98$ (Fig. S5 and Fig. 7, black dotted traces), that is typical for heme iron in the ferric high-spin state. Upon reaction with *m*-CPBA a new and distinct EPR signal was observed: an axial and very broad (2000 G) EPR spectrum, extending between the two resonances with observed g-values of 3.80 and 1.99 (Figure 7, light green trace) that is consistent with the expected axial EPR spectrum of an exchange-coupled oxoferryl-porphyrin radical species, [Fe^{IV}=O $Por^{\bullet+}$] with $g_{\perp}^{eff} = 3.80$ and $g_{\parallel}^{eff} = 1.99$, as previously reported for the porpholactone ferryl radical complexes [74] and iron porphyrins that are highly nonplanar, but not ruffled.[45, 75] The fact that this new broad and axial EPR signal could only be detected at temperatures lower than 30 K (due to line broadening effect [76]), well agrees with the expected behavior of a radical in magnetic interaction (exchange-coupling) with the ferryl moiety. Interestingly, the EPR spectrum is virtually identical, including the overall width (ca. 250 G) of the resonance at g = 3.80 ($g_{\perp}$) and the narrow and asymmetric resonance at g = 1.99 ($g_{\parallel}$), to that of the previously reported [Fe^{IV}=O $Por^{\bullet+}$] intermediate of nitrophorin, a heme-containing enzyme showing substantial peroxidase-like activity.[77] When thawing and incubating the EPR sample during 15 min at 20°C, the resulting EPR spectrum (Fig. 7, dark red trace) showed the complete disappearance of the broad axial signal of the [Fe^{IV}=O $Por^{\bullet+}$] species, as expected if considering the short-lived character of this intermediate demonstrated by the stopped-flow electronic absorption experiments (Fig. S3A, red trace).

View Article Online
DOI: 10.1039/C9SC04388H

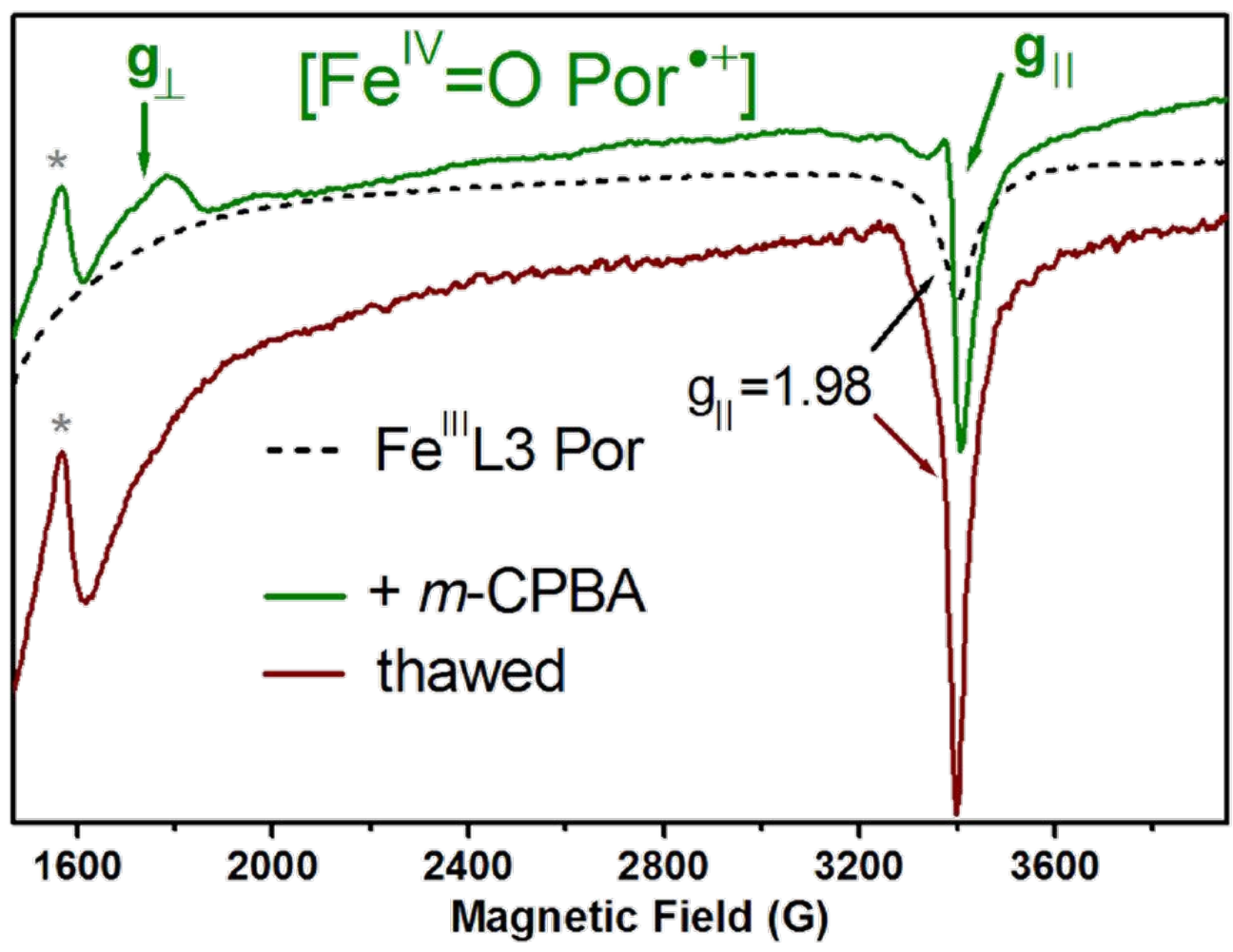

Figure 7. The 4K 9-GHz EPR spectra of the [Fe^{IV}=O $Por^{\bullet+}$] intermediate (light green trace) trapped when reacting the Fe^{III}L3 porphyrin complex (black dotted trace, 80 µl at 1.1mM initial concentration) with *m*-chloroperbenzoic acid (20 µl at 50 mM initial concentration), both in dichloromethane and during 3s in a cold bath (at ca. -100 °C) prior to flash freezing in liquid nitrogen. The final *molar* excess for the *m*-CPBA oxidant was 10 folds. When thawing the reacted sample (light green trace) during 15 min at 20°C, spectral changes were clearly observed (dark red trace). The ferric EPR spectrum of the Fe^{III}L3 porphyrin complex, emulating the contribution of the non-converted complex upon reaction with m-CPBA (dotted black trace), is also plotted to better illustrate the expected difference between the g ≈ 2 components of the ferric and the [Fe^{IV}=O $Por^{\bullet+}$] intermediate. EPR spectra (3 scans) were recorded at 4 K, 9.48 GHz frequency, 13 G modulation amplitude, 1 mW microwave power, and 100 KHz modulation frequency. The asterisk (*) shows the contribution of free iron (g = 4.3).

Compound II, the reaction intermediate (absorption CT band at 657 nm) formed subsequently to the Compound I in the stopped-flow absorption experiments is an integer spin species ([Fe^{IV}=O]), thus EPR-silent. The fact that the EPR signal of the trapped [Fe^{IV}=O $Por^{\bullet+}$] species does not fully account for the conversion of the ferric signal upon reaction with *m*-CPBA (as estimated by the decrease of the ferric EPR signal; see Fig. S5) is

View Article Online
DOI: 10.1039/C9SC04388H

fully consistent with the subsequent formation of the oxoferryl intermediate, an EPR-silent species. In addition, the higher stability of this intermediate, as shown by the stopped-flow experiments (Fig. S3A, green trace), is consistent with the partial recovery of the ferric signal , reflected by the increase of its $g_{||} = 1.98$ component (Fig.8, dark red trace and Fig. S5, dark green trace) when thawing the EPR sample during 15 min at 20°C (see above). Further thawing and incubation of the sample (at 20°C during 60 min) showed a small further increase in the intensity of the ferric signal (see Fig. S6), thus confirming that the [Fe^{IV}=O] species is rather stable at room temperature, as previously reported for natural peroxidases. For example, in the case of the bi-functional peroxidases KatGs, the [Fe^{IV}=O $Por^{\bullet+}$] species is very short-lived while the [Fe^{IV}=O] intermediate converts back to the ferric resting state only after 12 min at 20°C, and provided that all the oxidant has been used up.[78] This implies that the distal hydrogen bonding stabilizes the oxoferryl intermediate.

It is of note that Dawson and coworkers, using rapid-scan stopped flow absorption spectroscopy, reported that *m*-CPBA can play both the roles of oxidant and substrate in the formation of the catalytic intermediates of *C. fumago* chloroperoxidase.[79] It was concluded that *m*-CPBA acts as oxidant in the conversion of the ferric enzyme to the Compound I intermediate, and also as one-electron donor (i.e. 'substrate') in the subsequent reductions of Compound I to Compound II, and of Compound II back to ferric native enzyme.[79] In the case of the Fe^{III}L3 porphyrin complex reacted with *m*-CPBA, further incubation at -100°C during 3 s, showed an increase of the ferric EPR signal and no detectable change of the [Fe^{IV}=O $Por^{\bullet+}$] EPR signal (Fig. S6). This result can be rationalize as the reaction of the [Fe^{IV}=O] intermediate with the remaining *m*-CPBA, as in the case of chloroperoxidase. It is of note that intramolecular e^- transfer reactions can readily happen at such low temperatures.[78] Taken together, these EPR experiments confirm that the [Fe^{IV}=O $Por^{\bullet+}$] intermediate formed by the peroxidase-like reaction (Compound 0-Compound I) of the Fe^{III}L3 porphyrin complex with *m*-CPBA is a short-lived species even at subzero temperatures, and that the subsequent intermediate, the [Fe^{IV}=O] species (Compound II), formed most possibly by the reaction of the [Fe^{IV}=O $Por^{\bullet+}$] intermediate with *m*-CPBA, is relatively stable at room temperature. In addition, the [Fe^{IV}=O] intermediate can react slowly with *m*-CPBA as one-electron donor, resulting in a partial cycling back to ferric resting state.

The Compound I formed in most synthetic (ferric) iron porphyrin complexes, readily attacks the meso position of the porphyrin macrocycle leading to the formation of a isoporphyrin, an intermediate leading to the eventual degradation of the iron porphyrin complex (scheme S1). Accordingly, the UV-vis absorption spectrum of Fe^{III}TPP(Br) upon reaction with *m*-CPBA showed the appearance of the broad absorption bands at 800-900 nm (Figure 5, red trace & Figure S2) consistent with the isoporphyrin species. At variance, Fe^{III}L2(Br) and Fe^{III}L3(Br) complexes show very minor formation of isoporphyrin (Figure 5A and 5B, violet and green traces in Figure 5B) and converted to Compound II then eventually cycled back to the ferric complex, as indicated by UV-Vis spectra and consistent with the EPR spectroscopic characterization (see above). These results suggest that not only the basic groups in Fe^{III}L2 and Fe^{III}L3 accelerate the heterolysis of the peroxide inciting the formation of Compound

View Article Online
DOI: 10.1039/C9SC04388H

I, but also decelerates the electrophilic attack of Compound I on the porphyrin ring. This attribute implies that $Fe^{III}L2(Br)$ and $Fe^{III}L3(Br)$ should be able to catalyze oxidation of substrates by *m*-CPBA.

Catalytic Oxidation of Substrates

The reaction of $Fe^{III}L2(Br)$ and $Fe^{III}L3(Br)$ with *m*-CPBA in the presence of excess ferrocene (Fc) as an external sacrificial electron donor was monitored. The formation of a new band at 620 nm, characteristic of ferrocenium (Fc^+), indicates oxidation of ferrocene by the porphyrin complexes (Figures 8 and S7). In the presence of excess ferrocene and *m*-CPBA, both $Fe^{III}L2$ and $Fe^{III}L3$ can catalyze its oxidation with turnover numbers (TON) of 67 and 96, respectively, and turnover frequency (TOF) of 2.68 s^{-1} and 6.40 s^{-1}, respectively (Table 2). The catalytic turnover entails oxidation of two molar equivalents of ferrocene per Compound I species, i.e. Compound I + 2Fc → $Fe^{III}L$ + 2Fc^+ (Scheme 1). This result is expected, as E^o of Fc is lower than both Compound I and Compound II. Similarly to the case of peroxidases, the organic substrate 2,4,6-tri tertiarybutyl phenol (TBPH) is oxidized to the corresponding phenoxy radical, as shown by the absorption spectra with bands at 380 nm, 400 nm and 625 nm (Figure S7B) and the EPR spectrum measured at 77K showed a signal at g=2 consistent with an organic radical (Figure S8A).[80] Both $Fe^{III}L2(Br)$ and $Fe^{III}L3(Br)$ can catalyze the oxidation of TBPH with TON of 25 and 350, respectively, with TOF of 1.41 s^{-1} and 0.63 s^{-1}, respectively (Table 2). Similarly, the two-electron oxidation of o-phenylene diamine (OPD) to 2,3-diaminophenazine with characteristic absorption feature at 450 nm for these two iron porphyrins (Figure S10) yields TON of 68, 61, respectively, and the corresponding TOF are 0.85 s^{-1}, 2 s^{-1}, respectively. Note that these are the first examples of catalytic oxidation of phenol and amines by one electron (normal peroxidase activity) by synthetic heme complexes using peracid as oxidant.

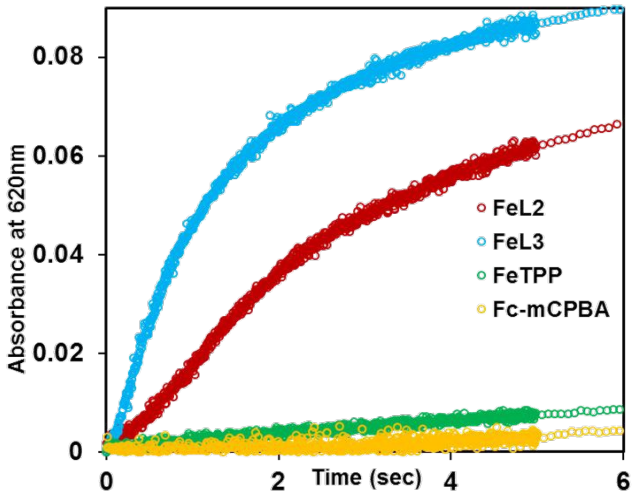

Figure 8. The time traces in rapid scan stopped flow kinetics measurement of $Fe^{III}L2(Br)$, $Fe^{III}L3(Br)$, $Fe^{III}TPP(Br)$ complexes and substrate (fc) with *m*-CPBA in dichloromethane at -30°c in a cuvette of 1cm path length with and without catalyst for formation of ferrocenium at 620 nm by the addition of iron-porphyrins (4 μM) with *m*-CPBA (500 eq, 1 mM) and ferrocene (500 eq, 2 mM).

View Article Online
DOI: 10.1039/C9SC04388H

Table 2. Catalytic Substrate oxidation

Substrate (2 mM)	$Fe^{III}L2(Br)$ (4 µM)		$Fe^{III}L3(Br)$ (4 µM)	
	TON[a]	TOF (s^{-1})[b]	TON[a]	TOF (s^{-1})[b]
Ferrocene (Fc)[c]	67	2.68	96	6.40
2,4,6-tri tertiarybutyl phenol (TBPH)[d]	25	1.41	350	0.63
o-phenylene diamine(OPD)[d]	68	0.85	61	2

a. The maximum number of product molecules obtained from per mole of catalyst.

b. TON at per unit time(sec)

c. Stopped flow kinetics at -30°c, d. UV-visible kinetic measurements at room temperature. The other conditions are described in the experimental section.

View Article Online
DOI: 10.1039/C9SC04388H

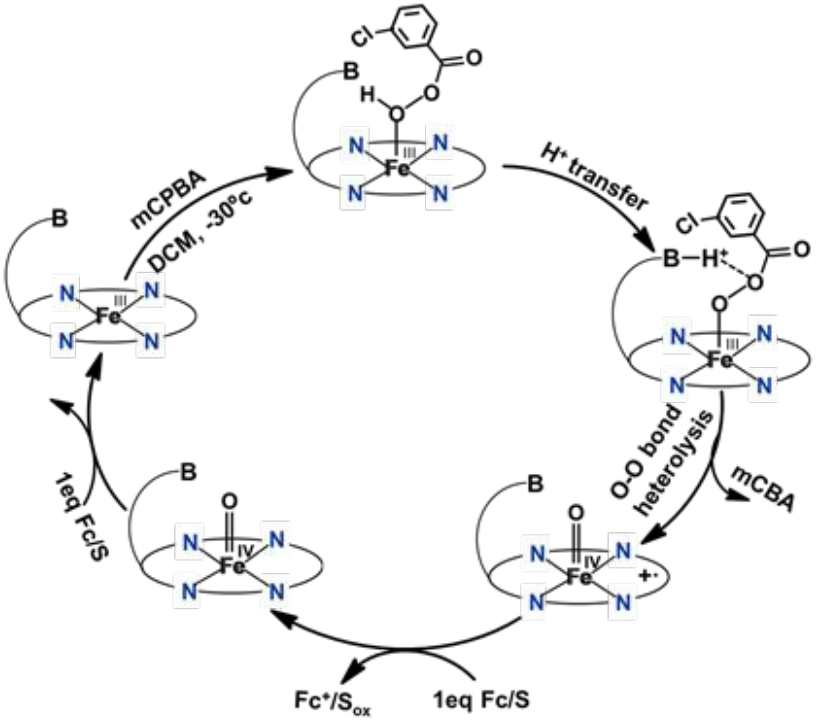

Scheme 1. Proposed mechanism of the catalytic cycle for the regeneration of high spin $Fe^{III}L2$ and $Fe^{III}L3$ via high valent intermediates starting from iron(III)-porphyrins in presence of meta-chloroperbenzoic acid (oxidant) and Ferrocene or any other one-electron donor/substrate (S) in dichloromethane at -30°C.

DFT Calculation

Having shown that facile O-O heterolysis in $Fe^{III}L2(Br)$ and $Fe^{III}L3(Br)$ allows rapid formation of Compound I which at its turn can oxidize ferrocene and TBPH, we performed DFT calculations to gain theoretical insight into the effect of pendent basic groups covalently attached to iron-porphyrins in relation to such O-O bond cleavage. The structures of *m*-CPBA bound metal complexes are optimized in PCM model using dichloromethane as solvent. In general, all attempts of optimizing the peracid bound ferric state inevitably leads to spontaneous O-O heterolysis forming Compound I and the *m*-chloroperbenzoic acid (Figure 9) likely due to the acidic proton of mCPBA (pKa=7.5 in water). Alternatively, the electronic structure contribution of the pendent basic groups to O-O bond heterolysis can be evaluated with H_2O_2 which has a higher pKa (11.75). Note that the use of hydrogen peroxide is more relevant to the chemistry of peroxidases. The structures with hydroperoxide bound resulting in low spin ferric porphyrins with protonated pendent basic groups, are optimized (Figure S11). In case of $[Fe^{III}L2\text{-}OOH]H^+$, the $-N_1H$ group and protonated pyridine (N_2H^+) acts as a H-bond donor to the distal oxygen atom. The optimized geometry shows that the O-O bond length for $[Fe^{III}L2\text{-}OOH]H^+$ is elongated to 1.88 Å in the protonated structure (Figure S11) which is much longer than that of Fe^{III}TPP-OOH (the O-O bond length is 1.46 Å) and free H_2O_2.[59]

View Article Online
DOI: 10.1039/C9SC04388H

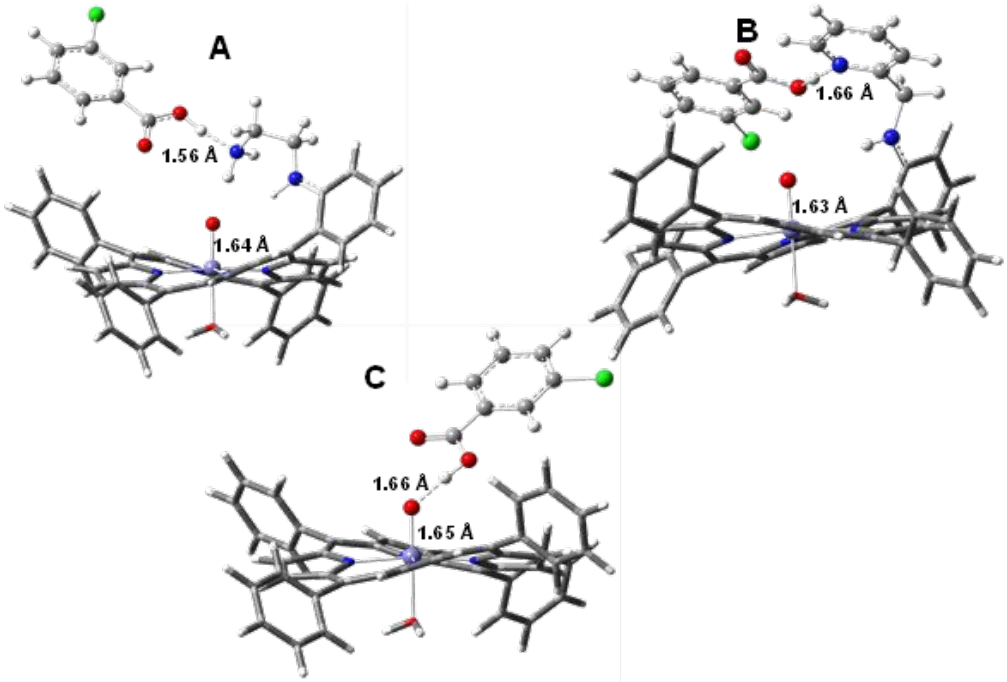

Figure 9. Optimized structures of six coordinate low spin (A) [Fe^{III}L3-*m*-CPBA]H^+; (B) [Fe^{III}L2-*m*-CPBA]H^+; (C) [Fe^{III}TPP-*m*-CBPA]H^+ with *m*-CPBA and water as axial ligands and distal basic groups in PCM model considering CH_2Cl_2 as solvent. *color codes*: carbon → *grey*, hydrogen→ white, nitrogen → *blue*, oxygen → *red*, chlorin → green and iron → *bluish grey*.

The same trend also occurs for protonated Fe^{III}L3-OOH, where the protonated aliphatic amine group (-NH_3^+) elongates the O-O bond length to 1.86 Å (Figure S11). All these optimized geometries suggest that strong H-bond donation to the distal oxygen atom of the Fe^{III}-OOH species facilitate activation of the O-O bonds. These appended groups in the studied porphyrin complexes appear to be oriented in such a way to allow selective delivery of protons to the distal oxygen atom with simultaneous weakening of the O-O bond, both factors beneficial for heterolytic O-O bond cleavage.[59]

The substantial activation of the O-O bond of a Fe^{III}-OOH species with H-bonding by a protonated base is the root of the "pull effect" proposed in peroxidase active sites where an analogous Fe^{III}-OOH species is produced, Compound 0.[24, 81, 82] The DFT calculated wave functions show that the Fe dπ character in the O-O σ* orbitals increase from 4.86% in the non H-bonded system to 36.89% and 38.69% in porphyrins having protonated OOH]H^+, respectively (Figure 10).

View Article Online
DOI: 10.1039/C9SC04388H

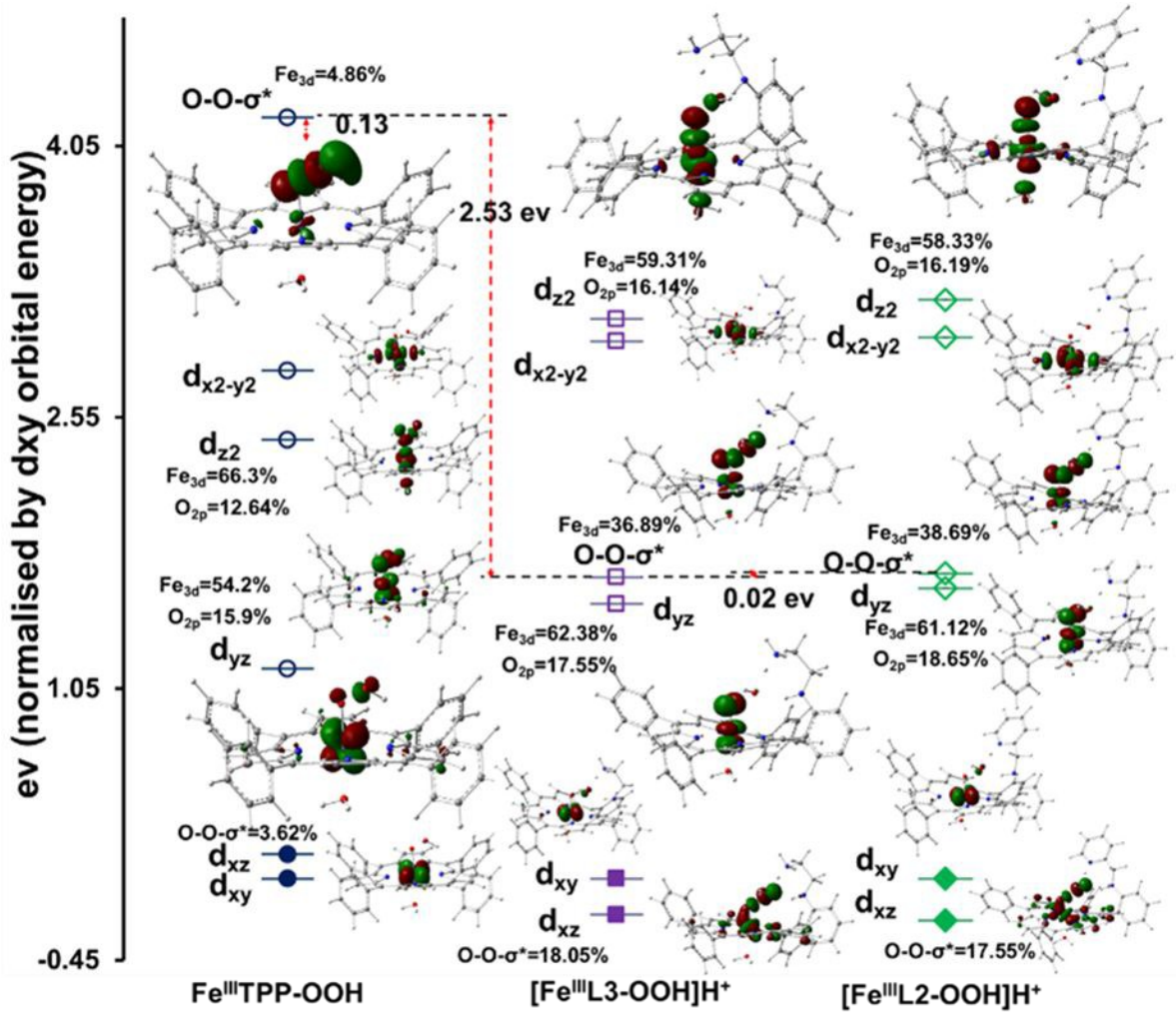

Figure 10. Calculated (BP86) ground state MO diagram of Fe(III)TPP-OOH (no H-bonding residue), [Fe(III)L3-OOH]H^+) and [Fe(III)L2-OOH]H^+ (protonated H-bonding residue). The relative energies are normalized with respect to the non-bonding d_{xy} orbital. Only β orbital are shown. The orbital contributions of occupied d_{xz} orbital and the unoccupied O-O σ* orbital are shown. The contributions of d_{z2} and the d_{yx} orbitals of the Fe that σ and π bonds, respectively, to the hydroperoxide are also shown. The non-bonding d_{xy} and the d_{x2-y2} are not shown for clarity.

The enhanced back-bonding is facilitated by the lowering of the O-O σ* orbital energies due to hydrogen bonding to the pendent basic groups for [Fe^{III}L3-OOH]H^+ and [Fe^{III}L2-OOH]H^+ group (Figure 10) which polarize the electron density of the O-O bond towards the distal OH group reducing the overlap between the two O_{2p} orbitals and lowering the energy of the O-O σ* orbital. This polarization is magnified when the amines are protonated. This is evident from the calculated Mulliken charge density on distal oxygen atom for [Fe^{III}L3-OOH]H+ (Op=-0.30, Od=-0.60) and [Fe^{III}L2-OOH]H+ (Op=-0.29, Od=-0.61) which is more negative than the Fe^{III}TPP analogue (Op=-0.293, Od=-0.383) without any hydrogen bonding residue (Figure S12). Thus the "pull effect" in this case may be interpreted as *pulling the energy of the O-O σ* orbital down* substantially by hydrogen bonding to a

View Article Online
DOI: 10.1039/C9SC04388H

protonated basic residue to allow better back-bonding into the O-O σ* orbital from filled Fe dπ orbital of the metal. The O_{2p} coefficient increases from 3.62% in Fe^{III}TPP-OOH to 18.05% in [Fe^{III}L3-OOH]H+ and 17.55% in [Fe^{III}L2-OOH]H+ in the dπ orbital signifying increased covalent donation from the proximal oxygen to the empty Fe dπ orbital i.e. strong π bonding (Figure 10). Similar increase in σ covalency is observed in the d_{z2} orbital. These are consistent with the shortening of Fe-O bond upon elongation of the O-O bond taking the reactant Fe^{III}-OOH to the product [Fe(IV)=O Por$^{\bullet+}$].

In nature, the alternative mechanism of activating a Fe^{III}-OOH used in Cyt P450 and CPO is the "push effect" of an axial thiolate ligand. The anionic thiolate ligand enhances the electron density of its trans axial ligand increasing the basicity. This enhanced pKa (~12) leads to a protonated compound II in Cyt p450/CPO when Compound II is deprotonated in peroxidases/Myoglobin with a pKa of around 3.[83, 84] DFT calculations on a hypothetical thiolate bound Fe^{III}TPP-OOH species show a O-O bond length of 1.46 Å which is shorter than [Fe^{III}L2-OOH]H$^+$ with protonated pendent base (1.88Å) and the Fe-O bond length of thiolate bound Fe^{III}TPP-OOH is calculated to be 1.85Å which is shorter than that of [Fe^{III}L2-OOH]H$^+$ (Figure S11). The Mulliken charge on the hydroperoxide unit of the thiolate bound Fe^{III}TPP-OOH species is calculated to be Op=-0.362 and Od=-0.422. The negative charge of the distal oxygen atom of the bound hydroperoxide is substantially more negative than a Fe^{III}TPP-OOH without axial thiolate (Op=-0.293, Od=-0.383) (Figure S12). The MO diagram of the thiolate bound Fe^{III}TPP-OOH shows much less electron donation by the bound –OOH to the Fe dσ and dπ orbitals consistent with greater anionic charge on the bound hydroperoxide relative to Fe^{III}TPP-OOH. There is very little Fe_{3d} character in the O-O σ* suggesting the lack of back-bonding from the filled Fe_{3d} consistent with the short O-O distance (Figure S13). Thus the "push effect" of the thiolate is limited to push electron density to the bound –OOH ligand increasing its basicity causing its protonation at physiological pH (Figure 11). Once protonated, the resulting Fe^{III}-OOH_2^+ species will have a very weak O-O bond which would cleave almost spontaneously. Alternatively, the "pull effect" of the pendent basic group results from polarization of the electron density of the peroxide resulting in lowering the O-O σ* energy (Figure 11) which allows greater back-bonding into the O-O σ* from the filled 3d orbitals of the iron due to better energy match and thus, weakening of the O-O σ bond activates the O-O bond for cleavage.

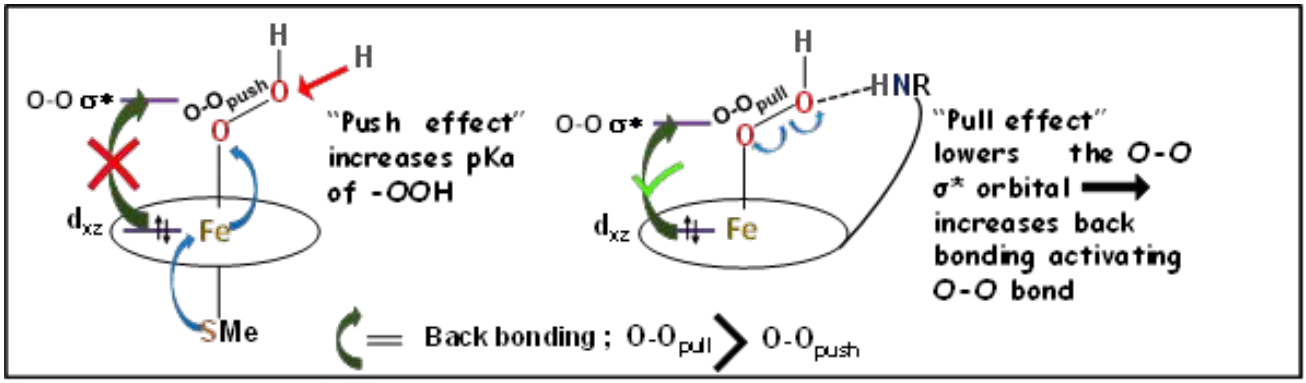

View Article Online
DOI: 10.1039/C9SC04388H

Figure 11. Schematic representation of O-O bond activation by "push effect" and "pull effect".

Conclusion

Inclusion of pendent basic groups in iron porphyrins, mimicking the 2nd sphere interactions present in the distal site of HRP, enables facile O-O bond heterolysis of peracids having barriers lower than naturally occurring enzymes. The Compound I generated by these iron porphyrin complexes with 2nd sphere coordination, is capable of oxidizing two equivalents of substrates (both organic and inorganic) thus making them functional models of natural peroxidases. The introduced basic groups, mimicking the His-Arg base pair in the active site of horseradish peroxidase, not only enable facile heterolysis but also stabilize the Compound I and Compound II intermediates. More importantly, electrophilic attack to the porphyrin macrocycle is prevented and such intermediates effectively oxidize organic and inorganic substrates, using an outer-sphere electron transfer mechanism. Accordingly, these synthetic complexes act as efficient catalysts with reasonable TON and TOF. Investigations are underway to understand how the hydrogen bonding tunes the reactivity of the high valent oxoferryl species from electrophilic inner-sphere oxidation (monooxygenase-like) to outer-sphere electron transfer (peroxidase-like).

Experimental Procedures

Instrumentation: All UV-Visible absorption spectra were recorded on an Agilent 8453 diode array spectrophotometer in a cuvette of 1 cm path length at room temperature unless otherwise mentioned. Rapid mixing Stopped flow kinetics were performed in SFM 4000 spectrophotometer (Halogen-deuterium lamp as light source) equipped with a low temperature chamber. The 4K 9-GHz EPR spectra were recorded on a Bruker EleXsys E500 spectrometer equipped with a standard Bruker ER4102 X-band resonator and a liquid helium cryostat (Oxford Instruments, ESR 900). EPR quartz tubes of 4 mm external diameter were used. A JEOL FA200 spectrometer was used for the measurements at 77K.

Materials: All reagents were of the highest grade commercially available and were used without further purification. The iron-porphyrins (Fe^{III}L2(Br), Fe^{III}L3(Br) and Fe^{III}TPP(Br)) studied here were synthesized according to previously reported procedures.[59] 3-Chloroperoxybenzoicacid (*m*-CPBA) was purchased from Aldrich (77%) and purified by washing with pH 7.40 phosphate buffer and recrystallization from pentane to remove 3-chlorobenzoic acid. Purity (>95%) was determined by 1H NMR. Solvents were purchased from RANKEM with HPLC grade for spectroscopic purpose. 2,4,6-tritertiary butyl phenol (TBPH), Ferrocene (Fc) were also purchased from Sigma-Aldrich.

Synthesis:

1a. Mono benzyl substituted monoamino porphyrin (MPh): The synthetic strategy utilized *o*-aminophenyl-tris(phenyl)-porphyrin (**MAPP**) as starting material.[85] To 20 ml solvent mixture of THF-acetonitrile (1:3), **MAPP** (50mg, 0.079mmol) was added. Then, benzaldehyde (30µl, 0.316mmol) and trifluoroacetic acid (28µl,

View Article Online
DOI: 10.1039/C9SC04388H

0.371mmol) were added to the solution and turned green. After 2hr, 5 equivalent of $NaBH_4$ (16mg, 0.417mmol) was added to the reaction and was further, stirred for 12 hr. The colour again changed to reddish brown. The solvent was removed through rotary evaporator and the compound was extracted with dichloromethane. The organic layer was dried with Na_2SO_4 and the solvent was evaporated to isolate the compound. Then the desired compound was eluted with 50% DCM-hexane mixture through column chromatography using neutral alumina and purple coloured solid was isolated (**Mph**, Scheme S2). Yield: (45 mg, 80%); ^{1}H NMR (500 MHz,$CDCl_3$, 25°C): δ, ppm = 9.03 (m, 8H), 8.30 (d, 6H), 7.95(d, 1H), 7.83(m, 9H), 7.66(t, 1H), 7.13(m, 7H), 7.05(m, 2H), 4.55(d, 2H), 3.88(t, NH), -2.62(s, 2H); UV-Vis (CH_2Cl_2): λ_{max}= 418nm, 516nm, 551nm, 591nm, 651nm ; ESI-MS (positive ion mode in ACN): *m/z* (%) = 720.29 (100) $[MPh]H^+$

1b. Mono benzyl substituted monoamino iron porphyrin [Fe^{III}MPh(Br)]: The ligand (50mg, 0.069mmol) was dissolved in dry degassed THF and about 18µl of collidine was added to it and stirred for 5minutes. Then $Fe^{II}Br_2$ (60mg, 0.276mmol) was also added and stirred, overnight. After the completion of the reaction the solvent was removed and the reaction mixture was worked up with DCM after treating with dil. HCl to remove excess $FeBr_2$. The organic layer was dried over anhydrous Na_2SO_4 and evaporated using a rotary evaporator. The reddish brown colored solid was isolated (**Fe^{III}MPh(Br)**, Scheme S2). Yield: (51 mg, 95%); Elemental analysis calcd (%) for $[Fe^{III}L2]Br$ ($C_{51}H_{35}BrFeN_5.C_6H_{14}$): C 72.85, H 5.26, N 7.45; Found: C 73.46, H 5.34, N 7.89; ^{1}H NMR (500 MHz, $CDCl_3$, 25°C): δ, ppm = 79.70 (pyrrolic protons), 12-14 (meta hydrogens of phenyl rings of the porphyrin); UV-Vis (CH_2Cl_2): λ_{max}= 417nm, 510nm, 584nm, 660nm and 696nm. ESI-MS (positive ion mode in ACN): *m/z* (%) = 773.23 (100) $[Fe^{III}MPh]$.

2a. UV-Visible absorption kinetics of substrate oxidation: In a cuvette containing 2ml dichloromethane, iron porphyrin (8µl, 1mM), *m*-CPBA (40µl, 50mM) and TBPH (40ul, 100mM) were added result in a final ratio of the mixture as Catalyst : *m*-CPBA : TBPH = 1:250:500. The kinetics were recorded at room temperature and using a time interval of 0.5sec. Oxidation of TBPH to 2,4,6-tri tertiary butyl phenoxyl radical (TBP) was monitored using the time traces of the characteristic absorption bands at 380nm, 400nm and 635nm. Similar conditions are applied for OPD oxidation to the corresponding 2,3-diaminophenazine formation with absorption feature at 450 nm.

2b. Stopped Flow Kinetics: In order to measure the rapid kinetics for Compound I formation, a cuvette of 1cm path length was used. One gastight syringe was filled with the porphyrin compound (50 µM, 3 ml) and the other with *m*-CPBA (200 µM, 5ml) in dichloromethane. Then the solutions were loaded into spectrophotometer and triggered by simultaneous injection of each solution according to the required ratio of compound and oxidant. The solutions were cooled to -30 °C prior to mixing and maintained in a chilled isopentane bath throughout the reaction.

The reactions with Ferrocene as a substrate were very rapid at room temperature and thus were performed in the stopped-flow set-up immersed in a cold bath (-30 °C). In a typical experiment, three syringes filled with ferrocene (2 mM, 3 ml), *m*-CPBA (1 mM, 5 ml) and iron porphyrin (4 µM, 2 ml), respectively, and volumes of these were

View Article Online
DOI: 10.1039/C9SC04388H

injected to achieve a final concentration ratios of 1:250:500 for iron porphyrins:*m*-CPBA: Ferrocene of the mixture.

2c. Fitting of kinetic data

$y = y0 + A0 \exp(-kt)$

or, $\log A0 = kt + \log(y-y0)$

The above first order monophasic equation was used to fit the kinetics data and thus obtained the first order rate constants of initial formation and decay from the slope of linear fit in logA0 vs time trace plot.

2d. TON Calculation: TON for substrate oxidation have been calculated with iron porphyrins (0.2 mol%) and oxidant like *m*-CPBA (Substrate:*m*-CPBA:catalyst = 1:250:500) from the ratio of oxidized product concentration with the initial catalyst concentration. For this purpose, we have determined the product concentration (c) from measured absorbance (A) and known molar extinction coefficient (ε) using the equation $A = \varepsilon * c * l$ (where, the path length of cuvette l = 1cm).

For ferrocenium hexafluorophosphate, molar extinction co-efficient (ε) value from the slope of absorbance vs concentration dependence plot (Figure S9) was obtained 350.34 $M^{-1}cm^{-1}$. The ε values 404 $M^{-1}cm^{-1}$ and 11.1 $mM^{-1}cm^{-1}$ for TBPH and OPD, respectively were obtained from an earlier report.[80, 86] TON is the number of substrate molecules oxidized into product by per mole of catalyst. TOFs have been calculated by dividing TON with the time required for maximum product conversion estimated at highest absorbance (Table 2). The TOF thus obtained represents an average rate over the entire duration of the reaction and not an initial rate.

3. EPR Spectroscopy and Sample Preparation : The EPR samples for the 4K measurements were prepared by manual mixing of 80 µL Fe^{III}L3 porphyrin complex dissolved in dichloromethane (initial concentration of 1.1 mM) with 20 µL of *m*-chloroperbenzoic acid (initial concentration of 50 mM), thus a final molar excess of 10 fold for the *m*-CPBA oxidant. The manual mixing of the complex with the oxidant was done directly in the 4 mm-EPR tube, kept in a cold bath of 2-methylTHF/liq N_2 (*ca.* -100°C). The mixing time was 3s, prior to flash freezing the sample in liquid nitrogen. It is of note that longer mixing times and/or higher temperatures resulted in a faster conversion of the [Fe^{IV}=O $Por^{\bullet+}$] to the [Fe^{IV}=O] intermediate.

In the case of samples used for the 77K EPR measurement of the TBP radical, samples were prepared in an EPR quartz tube using 80 µl of 2mM TBPH, 10 µl of 10mM *m*-CPBA and 10 µl of 44 µM FeL2/FeL3, so that the concentration ratios of the final resulting sample was 1:250:500 for iron porphyrins: *m*-CPBA:TBPH. The reaction mixture was kept in -80°C bath during 1min before flash freezing in liquid nitrogen.

4. DFT Calculation: The geometry of all compounds was optimized in gradient corrected BP86 Functional in unrestricted formalism using Gaussian 03 version C03. For hydroperoxide models, Fe, N and O atoms were optimised using 6-311G(d) basis set and 6-31G(d) for other all atoms. For *m*-CPBA bound models, the Fe, N and

View Article Online
DOI: 10.1039/C9SC04388H

O atoms were optimized using 6-311G(d) basis set and 6-31G(d) basis set for all other atoms in a Polarizable continuum model with dichloromethane.[87] The fully optimized structure is confirmed by doing their frequency calculation using same basis to ensure no imaginary mode is present for all these compounds. The final energy calculations were performed using 6-311+G(d) basis set on all atoms in PCM model using dichloromethane as solvent and convergence criterion of 10^{-10} Hartree.[88-90]

Acknowledgements

This work was funded by the Department of Science and Technology, India (EMR/2016/008063) and Council for Scientific and Industrial Research (CSIR) (to A.D.), the French National Center for Scientific Research (CNRS/UMR 7281) and the French EPR Federation/TGE RENARD (IR3443) (to A.I). S.B. and A.R. acknowledge IACS Integrated Ph.D. Programme for fellowships.

References

1. S. Chatterjee, K. Sengupta, B. Mondal, S. Dey and A. Dey, *Accounts of Chemical Research*, 2017, 50, 1744-1753.
2. S. M. Adam, I. Garcia-Bosch, A. W. Schaefer, S. K. Sharma, M. A. Siegler, E. I. Solomon and K. D. Karlin, *Journal of the American Chemical Society*, 2017, 139, 472-481.
3. M. Bhadra, J. Y. C. Lee, R. E. Cowley, S. Kim, M. A. Siegler, E. I. Solomon and K. D. Karlin, *Journal of the American Chemical Society*, 2018, 140, 9042-9045.
4. R. Cao, C. Saracini, J. W. Ginsbach, M. T. Kieber-Emmons, M. A. Siegler, E. I. Solomon, S. Fukuzumi and K. D. Karlin, *Journal of the American Chemical Society*, 2016, 138, 7055-7066.
5. K. Cheaib, M. Q. E. Mubarak, K. Sénéchal-David, C. Herrero, R. Guillot, M. Clémancey, J.-M. Latour, S. P. de Visser, J.-P. Mahy, F. Banse and F. Avenier, *Angewandte Chemie*, 2019, 131, 864-868.
6. A. W. Schaefer, M. T. Kieber-Emmons, S. M. Adam, K. D. Karlin and E. I. Solomon, *Journal of the American Chemical Society*, 2017, 139, 7958-7973.
7. L. Nurdin, D. M. Spasyuk, L. Fairburn, W. E. Piers and L. Maron, *Journal of the American Chemical Society*, 2018, 140, 16094-16105.
8. T. L. Poulos, *Chemical Reviews*, 2014, 114, 3919-3962.
9. A. Díaz, P. C. Loewen, I. Fita and X. Carpena, *Archives of Biochemistry and Biophysics*, 2012, 525, 102-110.
10. A. Ivancich and P. C. Loewen, *Electron Transfer in Catalases and Catalase-Peroxidases*, 2018.
11. E. J. Mueller, P. J. Loida and S. G. Sligar, in *Cytochrome P450: Structure, Mechanism, and Biochemistry*, ed. P. R. O. de Montellano, Springer US, Boston, MA, 1995, DOI: 10.1007/978-1-4757-2391-5_3, pp. 83-124.
12. A. W. Munro, K. J. McLean, J. L. Grant and T. M. Makris, *Biochemical Society Transactions*, 2018, 46, 183-196.
13. F. R. S. D. Keilin, T. Mann, *Proceedings of the Royal Society of London. Series B - Biological Sciences*, 1937, 122, 119.
14. F. L. Muller, M. S. Lustgarten, Y. Jang, A. Richardson and H. Van Remmen, *Free Radical Biology and Medicine*, 2007, 43, 477-503.
15. M. Zamocky, C. Jakopitsch, P. G. Furtmüller, C. Dunand and C. Obinger, *Proteins: Structure, Function, and Bioinformatics*, 2008, 72, 589-605.
16. S. Ghasempur, S.-F. Torabi, S.-O. Ranaei-Siadat, M. Jalali-Heravi, N. Ghaemi and K. Khajeh, *Environmental Science & Technology*, 2007, 41, 7073-7079.
17. O. Kirk, T. V. Borchert and C. C. Fuglsang, *Current Opinion in Biotechnology*, 2002, 13, 345-351.
18. Y. Watanabe, H. Nakajima and T. Ueno, *Accounts of Chemical Research*, 2007, 40, 554-562.
19. L. A. Blumenfeld, R. M. Davydov, N. S. Fel, S. N. Magonov and R. O. Vilu, *FEBS Letters*, 1974, 45, 256-258.
20. T. L. Poulos and J. Kraut, *Journal of Biological Chemistry*, 1980, 255, 8199-8205.
21. D. Dolphin, A. Forman, D. C. Borg, J. Fajer and R. H. Felton, *Proceedings of the National Academy of Sciences*, 1971, 68, 614-618.
22. T. Matsui, S.-i. Ozaki, E. Liong, G. N. Phillips and Y. Watanabe, *Journal of Biological Chemistry*, 1999, 274, 2838-2844.
23. A. N. P. Hiner, E. L. Raven, R. N. F. Thorneley, F. García-Cánovas and J. N. Rodríguez-López, *Journal of Inorganic Biochemistry*, 2002, 91, 27-34.
24. S.-i. Ozaki, M. P. Roach, T. Matsui and Y. Watanabe, *Accounts of Chemical Research*, 2001, 34, 818-825.
25. E. Derat and S. Shaik, *The Journal of Physical Chemistry B*, 2006, 110, 10526-10533.
26. J. N. Rodríguez-López, D. J. Lowe, J. Hernández-Ruiz, A. N. P. Hiner, F. García-Cánovas and R. N. F. Thorneley, *Journal of the American Chemical Society*, 2001, 123, 11838-11847.
27. J. E. Erman, L. B. Vitello, M. A. Miller, A. Shaw, K. A. Brown and J. Kraut, *Biochemistry*, 1993, 32, 9798-9806.
28. G. I. Berglund, G. H. Carlsson, A. T. Smith, H. Szöke, A. Henriksen and J. Hajdu, *Nature*, 2002, 417, 463.

View Article Online
DOI: 10.1039/C9SC04388H

29. B. D. Howes, J. N. Rodriguez-Lopez, A. T. Smith and G. Smulevich, *Biochemistry*, 1997, 36, 1532-1543.
30. T. L. Poulos, S. T. Freer, R. A. Alden, S. L. Edwards, U. Skogland, K. Takio, B. Eriksson, N. Xuong, T. Yonetani and J. Kraut, *Journal of Biological Chemistry*, 1980, 255, 575-580.
31. I. Fita and M. G. Rossmann, *Journal of Molecular Biology*, 1985, 185, 21-37.
32. M. Sundaramoorthy, J. Terner and T. L. Poulos, *Structure*, 1995, 3, 1367-1378.
33. J. N. Rodríguez-López, M. A. Gilabert, J. Tudela, R. N. F. Thorneley and F. García-Cánovas, *Biochemistry*, 2000, 39, 13201-13209.
34. S. Bhakta, A. Nayek, B. Roy and A. Dey, *Inorganic Chemistry*, 2019, 58, 2954-2964.
35. J. N. Rodriguez-Lopez, A. T. Smith and R. N. F. Thorneley, *Journal of Biological Chemistry*, 1996, 271, 4023-4030.
36. R. Nakajima and I. Yamazaki, *Journal of Biological Chemistry*, 1980, 255, 2067-2071.
37. S. Marklund, *Archives of Biochemistry and Biophysics*, 1973, 154, 614-622.
38. J. H. Dawson, *Science*, 1988, 240, 433.
39. Y. Watanabe and T. Ueno, *Bulletin of the Chemical Society of Japan*, 2003, 76, 1309-1322.
40. S. R. Bell and J. T. Groves, *Journal of the American Chemical Society*, 2009, 131, 9640-9641.
41. N. Jin, D. E. Lahaye and J. T. Groves, *Inorganic Chemistry*, 2010, 49, 11516-11524.
42. K. Yamaguchi, Y. Watanabe and I. Morishima, *Journal of the American Chemical Society*, 1993, 115, 4058-4065.
43. J. T. Groves and Y. Watanabe, *Journal of the American Chemical Society*, 1988, 110, 8443-8452.
44. J. T. Groves and Y. Watanabe, *Journal of the American Chemical Society*, 1986, 108, 7834-7836.
45. H. Fujii, T. Yoshimura and H. Kamada, *Inorganic Chemistry*, 1996, 35, 2373-2377.
46. J. D. Soper, S. V. Kryatov, E. V. Rybak-Akimova and D. G. Nocera, *Journal of the American Chemical Society*, 2007, 129, 5069-5075.
47. C. J. Chang, L. L. Chng and D. G. Nocera, *Journal of the American Chemical Society*, 2003, 125, 1866-1876.
48. F. Hollmann, P.-C. Lin, B. Witholt and A. Schmid, *Journal of the American Chemical Society*, 2003, 125, 8209-8217.
49. S. Shaik, S. Cohen, Y. Wang, H. Chen, D. Kumar and W. Thiel, *Chemical Reviews*, 2010, 110, 949-1017.
50. C. J. Thibodeaux, W.-c. Chang and H.-w. Liu, *Chemical Reviews*, 2012, 112, 1681-1709.
51. H. B. Dunford and B. B. Hasinoff, *Biochemistry*, 1970, 9, 4930-4939.
52. E. G. Hrycay and S. M. Bandiera, in *Monooxygenase, Peroxidase and Peroxygenase Properties and Mechanisms of Cytochrome P450*, eds. E. G. Hrycay and S. M. Bandiera, Springer International Publishing, Cham, 2015, DOI: 10.1007/978-3-319-16009-2_1, pp. 1-61.
53. M. I. Savenkova, J. M. Kuo and P. R. Ortiz de Montellano, *Biochemistry*, 1998, 37, 10828-10836.
54. J. T. Groves and T. E. Nemo, *Journal of the American Chemical Society*, 1983, 105, 5786-5791.
55. B. Meunier, *Chemical Reviews*, 1992, 92, 1411-1456.
56. X. Huang and J. T. Groves, *Chemical Reviews*, 2018, 118, 2491-2553.
57. T. G. Traylor, W. A. Lee and D. V. Stynes, *Journal of the American Chemical Society*, 1984, 106, 755-764.
58. T. G. Traylor and R. Popovitz-Biro, *Journal of the American Chemical Society*, 1988, 110, 239-243.
59. S. Bhunia, A. Rana, P. Roy, D. J. Martin, M. L. Pegis, B. Roy and A. Dey, *Journal of the American Chemical Society*, 2018, 140, 9444-9457.
60. I. Kaljurand, T. Rodima, I. Leito, I. A. Koppel and R. Schwesinger, *The Journal of Organic Chemistry*, 2000, 65, 6202-6208.
61. H. Fujii, *Journal of the American Chemical Society*, 1993, 115, 4641-4648.
62. I. Garcia-Bosch, S. K. Sharma and K. D. Karlin, *Journal of the American Chemical Society*, 2013, 135, 16248-16251.
63. S. Yokota and H. Fujii, *Journal of the American Chemical Society*, 2018, 140, 5127-5137.
64. W. D. Hewson and L. P. Hager, *Journal of Biological Chemistry*, 1979, 254, 3182-3186.
65. M. M. Palcic, R. Rutter, T. Araiso, L. P. Hager and H. B. Dunford, *Biochemical and Biophysical Research Communications*, 1980, 94, 1123-1127.
66. Z. Pan and M. Newcomb, *Inorg Chem Commun*, 2011, 14, 968-970.
67. Z. Pan and M. Newcomb, *Inorganic Chemistry*, 2007, 46, 6767-6774.
68. X. Lu, X.-X. Li, M. S. Seo, Y.-M. Lee, M. Clémancey, P. Maldivi, J.-M. Latour, R. Sarangi, S. Fukuzumi and W. Nam, *Journal of the American Chemical Society*, 2019, 141, 80-83.
69. Z. Cong, T. Kurahashi and H. Fujii, *Journal of the American Chemical Society*, 2012, 134, 4469-4472.
70. D. M. Davies, P. Jones and D. Mantle, *Biochemical Journal*, 1976, 157, 247-253.
71. S. L. Newmyer and P. R. O. de Montellano, *Journal of Biological Chemistry*, 1995, 270, 19430-19438.
72. T. L. Poulos, *Archives of Biochemistry and Biophysics*, 2010, 500, 3-12.
73. M. I. Savenkova, S. L. Newmyer and P. R. Ortiz de Montellano, *Journal of Biological Chemistry*, 1996, 271, 24598-24603.
74. K. Jayaraj, A. Gold, R. N. Austin, L. M. Ball, J. Terner, D. Mandon, R. Weiss, J. Fischer, A. DeCian, E. Bill, M. Müther, V. Schünemann and A. X. Trautwein, *Inorganic Chemistry*, 1997, 36, 4555-4566.
75. K. Ayougou, D. Mandon, J. Fischer, R. Weiss, M. Müther, V. Schünemann, A. X. Trautwein, E. Bill, J. Terner, K. Jayaraj, A. Gold and R. N. Austin, *Chemistry – A European Journal*, 1996, 2, 1159-1163.
76. J. T. Colvin, R. Rutter, H. J. Stapleton and L. P. Hager, *Biophysical Journal*, 1983, 41, 105-108.
77. R. Singh, R. E. Berry, F. Yang, H. Zhang, F. A. Walker and A. Ivancich, *Biochemistry*, 2010, 49, 8857-8872.
78. A. Ivancich, L. J. Donald, J. Villanueva, B. Wiseman, I. Fita and P. C. Loewen, *Biochemistry*, 2013, 52, 7271-7282.
79. D. P. Collins, I. S. Isaac, E. D. Coulter, P. W. Hager, D. P. Ballou and J. H. Dawson, *Journal of Porphyrins and Phthalocyanines*, 2013, 17, 63-72.

View Article Online
DOI: 10.1039/C9SC04388H

80. E. R. Altwicker, *Chemical Reviews*, 1967, 67, 475-531.
81. E. Derat, S. Shaik, C. Rovira, P. Vidossich and M. Alfonso-Prieto, *Journal of the American Chemical Society*, 2007, 129, 6346-6347.
82. H. K. Baek and H. E. Van Wart, *Biochemistry*, 1989, 28, 5714-5719.
83. K. L. Stone, R. K. Behan and M. T. Green, *Proceedings of the National Academy of Sciences*, 2006, 103, 12307-12310.
84. T. H. Yosca, R. K. Behan, C. M. Krest, E. L. Onderko, M. C. Langston and M. T. Green, *Journal of the American Chemical Society*, 2014, 136, 9124-9131.
85. J. P. Collman, J. I. Brauman, K. M. Doxsee, T. R. Halbert, E. Bunnenberg, R. E. Linder, G. N. LaMar, J. Del Gaudio, G. Lang and K. Spartalian, *Journal of the American Chemical Society*, 1980, 102, 4182-4192.
86. O. V Ignatenko, I. Gazaryan, E. A. Mareeva, T. A. Chubar, V. A. Fechina, P. Savitsky, A. M Rojkova and V. Tishkov, *Catalytic Properties of Tryptophanless Recombinant Horseradish Peroxidase*, 2000.
87. J. P. Perdew, *Physical Review B*, 1986, 33, 8822-8824.
88. S. Miertuš, E. Scrocco and J. Tomasi, *Chemical Physics*, 1981, 55, 117-129.
89. L. Noodleman and W.-G. Han, *JBIC Journal of Biological Inorganic Chemistry*, 2006, 11, 674-694.
90. M. G. Ullmann, L. Noodleman and D. A. Case, *JBIC Journal of Biological Inorganic Chemistry*, 2002, 7, 632-639.

View Article Online
DOI: 10.1039/C9SC04388H

TOC: